Study on Practical CFD for Unsteady Vortices from Trailing Edge of Propeller Blades

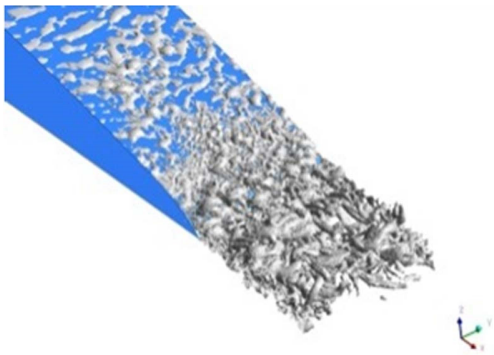

TAKUYOSHI YAMADA[*1] CHIHARU KAWAKITA[*2]

The reduction of underwater noise radiated from vessels and underwater vehicles prevents product problems and increases added value. One of the sources of underwater radiated noise is the propeller that produces the propulsion of a vessel or underwater vehicle. This article describes the method for analyzing the unsteady vortices that are generated around blades with high accuracy using CFD. Unsteady vortices cause singing noise among propeller noises. For the analysis method, ELES, which is a combination of RANS with a low calculation load and LES with a high calculation load, was used on understanding the ship-scale phenomenon with a relatively low calculation load. We chose the case in which the blade model was fixed in a uniform flow as the stage that precedes its application as a propeller. The general-purpose calculation domain decomposition method for ELES was constructed. We will develop low noise propellers by applying this method to propeller design.

1. Introduction

Recently, the effects of underwater noise radiated from vessels on marine life such as dolphins and whales have been perceived as a problem. Mainly in Europe, some regulations on underwater noise are being discussed by international organizations. So far, special vessels such as naval vessels, passenger ships and marine research vessels have been required to reduce underwater radiated noise. It is expected that general merchant vessels will also be increasingly required to reduce underwater radiated noise in the future.

The major causes of underwater radiated noise from vessels are: (I) mechanical noise caused by the propagation of vibrations from propulsion engines and auxiliary engines to outboard via hull structures; and (II) propeller noise. To deal with (I) mechanical noise, measures such as vibration control can be taken, but to mitigate (II) propeller noise, the noise produced by propeller itself needs to be reduced. Specifically, the development of a low noise propeller is needed.

(II) Propeller noise is broadly classified into three types: (II a) ship hull vibration noise caused by shaft force which is generated by the vibration of the ship's hull with shaft force with which the force/moment produced by the revolution of the propeller propagates to the ship's hull via the propeller shaft; (II b) ship hull vibration caused by surface force with which the fluctuating pressure wave from the propeller propagates to the shell plate of the ship's hull directly on propeller; and (II c) the flow noise arising from the fluctuation of the flow around propeller.

Furthermore, (II c) the flow noise of propellers is classified into three types: (II c-1) cavitation noise arising from propeller cavitation generated on the propeller blade surface; (II c-2) singing noise caused by resonance between vortex frequency at the trailing edge of the blade and the local natural frequency of the propeller blade; and (II c-3) turbulence noise arising from the fluctuation of vortices generated by the boundary layer of the blade surface and the fluctuation of vortices from the trailing edge of the blade. Among these types of flow noise, (II c-2) singing noise is caused by vortices, which were produced on the propeller blade surface and flowed into the trailing edge, vibrating the propeller blade. When the generation frequency of Karman vortices

*1 Fluid Dynamics Research Department, Research & Innovation Center, Technology & Innovation Headquarters
*2 Chief Staff Manager, Fluid Dynamics Research Department, Research & Innovation Center, Technology & Innovation Headquarters

generated at the trailing edge of the blade coincides with the local natural frequency of the propeller blade, a very large amount of underwater radiated noise is produced.

We are developing a method for analyzing vortices generated at the trailing edge of the blade in the flow at high Reynolds number through the fluid analysis using high resolution CFD (Computational Fluid Dynamics) for the ship-scale propeller. This article describes the unsteady vortices analysis method for propeller blade fixed in uniform flow which is in the pre-stage of application to propeller. CFD in this method uses ELES (Embedded LES), which is a kind of hybrid turbulence model formed by the combination of RANS (Reynolds-Averaged Navier-Stokes) model and LES (Large Eddy Simulation) model. This method enables a high-accuracy estimation of steady and unsteady vortices generated at the trailing edge of the blade at a calculation load applicable to the design.

2. Singing noise generation mechanism and estimation technologies

The cause of the generation of singing noise is the resonance phenomenon caused by the coincidence of the generation frequency of Karman vortices released from the trailing edge of the propeller blade with the natural frequency of the blade. **Figure 1** shows the state of Karman vortices generated at the trailing edge of the propeller blade. Karman vortices are formed in regular and alternating patterns in two rows at the trailing edge after the flow around an object is separated. As the vortices in two rows are formed in higher symmetry, the exciting force caused by the vortices increases. Two key technologies for estimating the generation of singing noise are as follows:

1) Estimation technology of vortices generated at the trailing edge of propeller blades
2) Estimation technology of natural frequency of propeller blades

Among the above two technologies, 2) Estimation technology of natural frequency of propeller blades has been established by the finite element method. Therefore, in order to improve the estimation accuracy of the generation of singing noise, it is necessary to improve the estimation accuracy of vortices generated at the blade trailing edge.

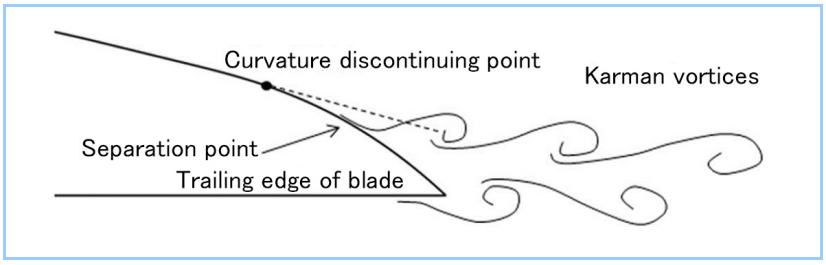

Figure 1 Karman vortices generated state
This shows the image of Karman vortices generated around the trailing edge of the blade. Karman vortices are formed in regular and alternating patterns in two rows from the separation point on the blade surface.

Figure 2 shows an example of the measurement of the flow velocity fluctuations near the blade trailing edge, which was conducted by Bourgoyne et al. using the two-dimensional cross sectional model (hereinafter referred to as a 2D blade) with the actual blade scale (blade chord length C=2.1336m) at the Large Cavitation Channel.[1,2] It shows the velocity power spectra (vertical blade flow velocity fluctuations) measured at 1% blade chord length downstream from the blade trailing edge (x/C=1.01), which is the flow velocity measurement position closest to the blade trailing edge. The measurement was conducted for several Reynolds numbers by changing the flow velocity in LCC. In the measurement results for the Reynolds number of 4×10^6, the velocity power spectrum is larger at the non-dimensional frequency (Strouhal number: Sh) of 0.2. Under this condition, it seems that strong Karman vortices are generated. A large velocity power spectrum means that the vertical blade velocity fluctuations at the blade trailing edge are large, specifically the exciting force to the blade is large. When this frequency coincides with the blade natural frequency, singing noise will be generated. When the Reynolds numbers are different, specifically when the flow states around the blade trailing edge are different even if the trailing edges have the same shape, strong Karman vortices may be generated. Therefore, in order to determine whether singing noise is generated, it is important to estimate the velocity field near the blade trailing edge with high accuracy.

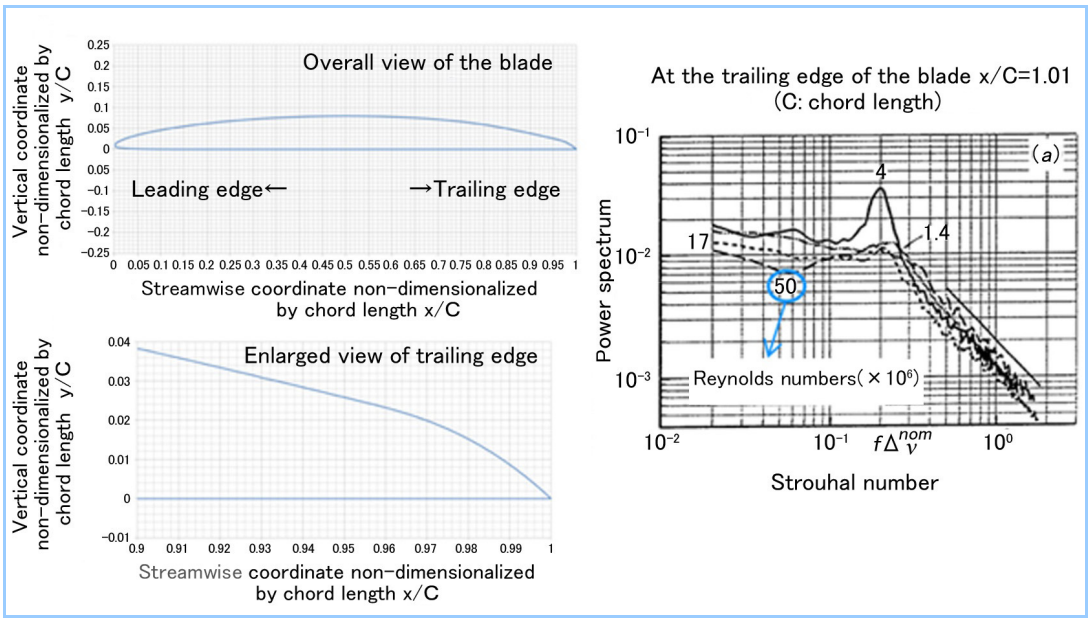

Figure 2 The blade section and spectra of vertical velocity measured at the Large Cavitation Channel[1, 2]

The results of the measurement at the trailing edge of the blade using a ship-scale blade model with a blade chord length of 2m have been published. The figure on the upper left shows the shape of the cross section of the blade and the figure on the lower left shows an enlarged view of the trailing edge, which is closely related to the generation of vortices. The figure on the right shows the measurement results of the vertical velocity power spectra at Reynolds numbers ranging from 4 x 10^6 to 50 x 10^6. In the case of a Reynolds number of 4 x 10^6, the peak occurs at the Strouhal number of 0.2. This peak is due to Karman vortices.

3. Comparison of the analysis methods for blade trailing edge vortices

At the blade trailing edge, in addition to large structural vortices such as Karman vortices, microscale vortices are also generated. For the analysis of such microscale vortices, it is considered that LES or DES (Detached Eddy Simulation) analysis is more suitable than unsteady RANS analysis. Therefore, we conducted the comparison calculation on the 2D blade which was used in the study by Bourgoyne et al. and investigated the effects of the difference of turbulence models on the calculation accuracy.

First, LES and DES analyses were conducted. For Re=4 x 10^6 (equal to the inflow velocity of 1.5m/sec) where strong Karman vortices are observed, the power spectra of vertical flow velocity fluctuations at 1% and 7% of the blade chord length downstream from the blade trailing edge were selected as the comparative verification data.

(1) Applicability of LES/DES analyses

Figure 3 shows the streamwise velocity distributions around the blade trailing edge obtained by RANS, LES and DES analyses. In LES analysis using the practical calculation load (the grid size is about 10 million) which is applicable to the design at this point in time, a problem was found in that the calculated boundary layer was underestimated. It seems to be a result of the lack of spatial resolution of the grid around the blade surface. Low resolution at the boundary layer which causes the reduction of calculation accuracy is a significant problem because vortices from the blade trailing edge are generated by turbulence in the boundary layer.

Therefore, we considered the application of DES, which is a kind of RANS-LES hybrid calculation method. In this model, we can analyze with LES at the calculation area where the turbulence length scale is large relative to calculation grid size and the other calculation area is calculated by RANS. DES determines the RANS/LES calculation area as a function of the distance from the wall. The vicinity of the wall is calculated by RANS, so that the thickness of the boundary layer shown in Figure 3 becomes the same as that by RANS, and the problem observed in LES where the boundary layer is underestimated was improved. On the other hand, only the area sufficiently downstream from the blade trailing edge is determined as the LES region, 1% of the blade chord length downstream from the trailing edge is insufficient as the LES region. For these reasons, it was determined that both LES and DES have less applicability to this analysis.

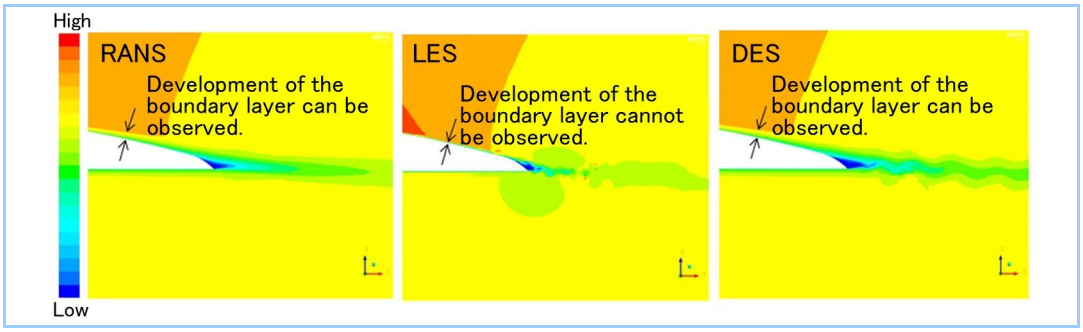

Figure 3 Comparison of the streamwise flow velocity distributions among turbulence models
Each figure shows the streamwise velocity distribution around the blade trailing edge. In RANS, the estimation accuracy of the boundary layer is high, and the thickness of the boundary layer increases toward the blade trailing edge. In LES, where the number of calculation grids is smaller, the estimation accuracy of the boundary layer is low and the development of the boundary layer cannot be observed. In DES, the estimation accuracy of the boundary layer is as high as in RANS.

(2) ELES analysis[3]

In ELES, the user sets any RANS region and LES region for divided calculation regions. Turbulence intensity data of the flow velocity calculated in the RANS region are transferred to the LES region, and the turbulence intensity component as vortices is converted to flow velocity fluctuation to set as the inlet boundary condition of the LES region.

Through the application of ELES to this analysis, LES is applicable to the area from the blade trailing edge to the blade downstream and RANS analysis is applicable to the area from the inlet boundary of the calculation area to the blade center. Thus, it is expected to improve both of the problems in LES and DES analysis, in which the boundary layer is underestimated in LES analysis, and microscale vortices are not calculated around the blade trailing edge in DES analysis.

4. ELES analysis method

ELES analysis was conducted with the following calculation conditions:

(1) Calculation grid

For the blade surface, small calculation grids were set only for the vicinity of the blade trailing edge with the spatial resolution of 0.1% of the blade chord length. For downstream from the blade trailing edge, the high resolution area which is 0.1% of the blade chord length was set over 10% of the blade chord length. In order to analyze the boundary layer with high accuracy, grids are arranged in the vicinity of the wall surface so that the non-dimensional minimum cell wall distance becomes y+=1.

The calculation region size in the streamwise and vertical direction are the same as the measurement section size described in the experiment report by Bourgoyne et al., and the upper and lower surfaces of the calculation region were set as the free slip wall boundary. The width size of the region was set only for 10% of the blade chord length, which is about 7% of the measurement area, and the infinite blade width was simulated with the side face boundary being set as the periodic boundary.

(2) Analysis code

The commercially available general-purpose fluid solver "Ansys Fluent 14.5" was used as the fluid analysis code, while Realizable k-ε Enhanced Wall Treatment model was used at the RANS region for the turbulence model. The WALE model was used as the subgrid scale model at the LES region, and Bounded Central Difference was used as the discretization scheme.

(3) Setting of calculation conditions

According to the report by Bourgoyne et al., the vertical component of flow velocity was measured, and the analysis resulted in the spectra $\Phi_v(f)$ (hereinafter, power spectra) which is the square of the vertical flow velocity fluctuation indicated in Equation 1.

The two measurement positions of the flow velocity in the streamwise direction are 1.0% and 7.0% of the blade chord length downstream from the blade trailing edge. The flow velocity observation positions in CFD were set at the same position in the measurement.

The time measurement position is 0.5 msec. The time series data of vertical velocity component are fed into a Fourier transform to compare the power spectra between measurement

and CFD. The range of time series data corresponds to the range in which unsteadiness was observed.

$$v'^2 / U_0^{\,2} = \left(\Delta_y / U_0\right) \cdot \int \Phi_v \mathrm{d}f \quad \cdots\cdots \text{Equation 1}$$

where, Δ_y is the representative length of Sh, which is a constant nominal wake thickness of 1% of the blade chord length. v' is the vertical flow velocity fluctuation component, U_0 is the inflow velocity, and f is the frequency in Hz.

5. Domain decomposition method in ELES analysis

5.1 Overview of domain decomposition

In ELES analysis, the user determines the RANS-LES interface, and RANS or LES is selected for two or more regions divided by the interface. Two domain decomposition cases for which the analysis was attempted are introduced as follows.[4]

(1) Domain decomposition A

The RANS region where the boundary layer can be resolved with high accuracy was arranged upstream of the blade surface and the LES region was arranged downstream from the vicinity of the curvature discontinuing point where vortices are generated. For the application of ELES, the RANS region and the LES region need to be separated. Therefore, as shown in **Figure 4**, the RANS region was set for the upstream side from the inflow boundary to 90% of the blade chord length, and the LES region was set for the downstream side from 90% of the blade chord length to the outflow boundary.

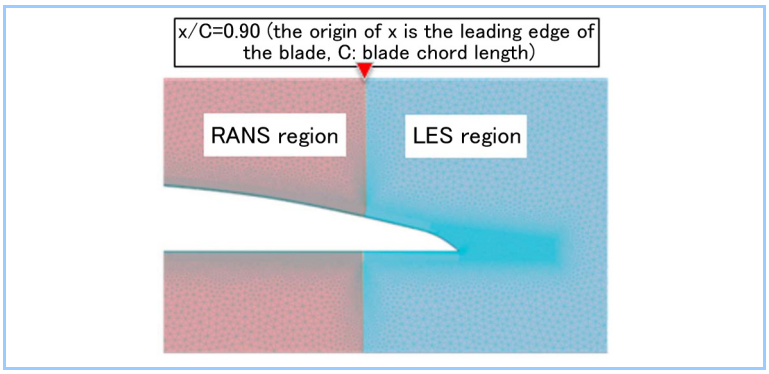

Figure 4 Divided region by domain decomposition A
The area is decomposed at 90% of the blade chord length. The upstream region was set for RANS, and the downstream region was set for LES

The distribution of the streamwise velocity component and the distribution of vortices around the blade trailing edge are shown in **Figure 5**. Using the RANS model for the analysis of the upstream side, the reduction of the boundary layer resolution was controlled, and using the LES model for the analysis of the vortices generated downstream from the separation, the unsteady vortices from the trailing edge of the blade could be resolved. Through the application of this method, it is expected that unsteady vortices can be resolved with high accuracy, at a calculation load which is applicable to the design.

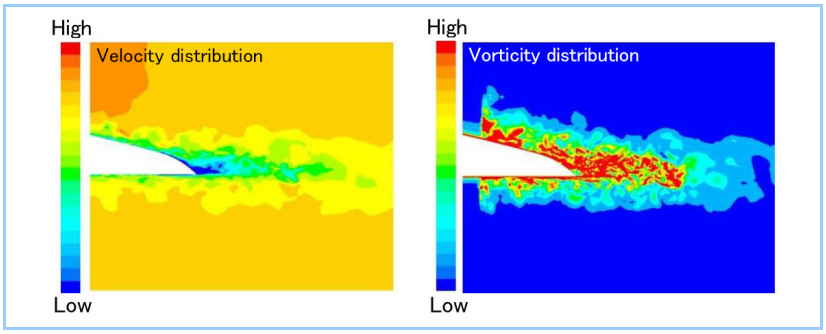

Figure 5 Analysis results of domain decomposition A (velocity distribution/vorticity distribution)
This shows the ELES analysis results in domain decomposition A. Microscale vortices have been analyzed. In the velocity distribution, the boundary layer thickness is analyzed as being thicker than the thickness in the results of LES (Figure 3). This indicates the improvement of accuracy. In the vorticity distribution, we can see the mottles around the trailing edge. That is, the microscale vortices downstream from the blade have been analyzed.

However, with this domain decomposition where the RANS-LES interface is arranged at 90% of the blade chord length, it is considered that the flexibility is reduced. When the attack angle or blade shape is changed, for example, the separation point is displaced and the area where vortices are generated is not always on the downstream side from 90% of the blade chord length.

(2) Domain decomposition B

In order to solve the problem in domain decomposition A, we studied the domain decomposition method in which the separation point and the area where vortices are easily generated are extracted based on the flow field analysis results for the RANS-LES interface, the inside of the area is set as LES, and the outside of the area is set as RANS. As the preliminary calculation for the extraction of the area which should be LES, DES analysis is conducted and the separation area produced at the trailing edge of the blade and Karman vortices generated downstream from the blade are analyzed.

The extraction methods of the separation area and the area for the passage of Karman vortices are described as follows.

[1] Separation area extracting method

It is considered that in the Karman vortices passage area, the fluctuations of the flow velocity are increased due to the passage of vortices, specifically the time fluctuations of the flow velocity are increased, and the area that meets the conditions of the determination equation $V_{\mathrm{mean}} < \frac{V_{\mathrm{in}}}{k}$ was determined as the Karman vortices passage area, where V_{mean} is the time averaged flow velocity, V_{in} is the outside flow velocity, specifically inflow velocity, and k is the empirically defined constant.

[2] Karman vortices passage area extracting method

It is considered that in the Karman vortices passage area, the fluctuations of the flow velocity are increased due to the passage of vortices, specifically the time fluctuations of the flow velocity are increased, and the area that meets the conditions of the determination equation $V_{\mathrm{rms}} > \frac{V_{\mathrm{in}}}{l}$ was determined as the Karman vortices passage area, where V_{rms} is the time fluctuated flow velocity, and l is the empirically defined constant.

By conducting DES analysis, the area where the flow velocity is reduced after separation at the blade trailing edge and the area where the time fluctuated flow velocity are increased after Karman vortices passed downstream from the blade can be extracted. **Figure 6** shows the time averaged flow velocity distribution and the time fluctuated flow velocity distribution. It shows that the area where the flow velocity is reduced in the flow velocity distribution in Figure 5 and the area close to the area where the vortices rate is increased in the vortices distribution in Figure 5 have been extracted.

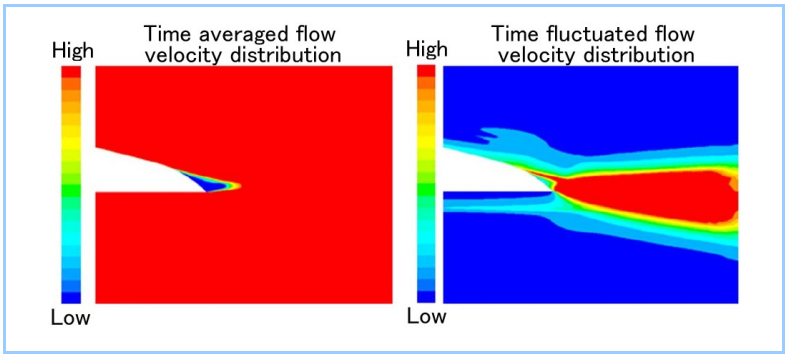

Figure 6 Analysis results of domain decomposition B which used fluid parameters for the decision of the RANS-LES interface

This shows the time averaged flow velocity (left) and the time fluctuated flow velocity (right) which are the fluid parameters used for the evaluation of area. In the area which may be determined as having been separated, the time averaged flow velocity is low (left). In the area where Karman vortices passed, the time fluctuated flow velocity is high (right). It is expected that the purpose of "the extraction of the area where vortices are generated downstream from the separation" can be achieved by the union of the separation area in the figure on the left and the area with large velocity fluctuations in the figure on the right.

The determined results of the LES region and the RANS region extracted by the time averaged flow velocity and the time fluctuations of the flow velocity are shown in **Figure 7**. The area shown in blue is the RANS region, while the area shown in red is the LES region. It shows that the separated downstream area which was proposed by domain decomposition B can be set as the LES region.

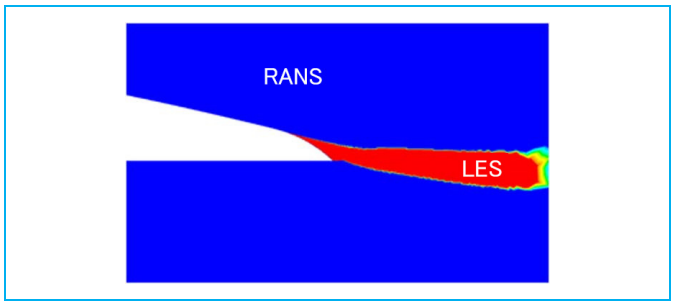

Figure 7 Decided region by domain decomposition B
This shows the decided region by the determination equation. This figure shows the union of the blue area (separation area) on the left in Figure 6 and the red area (highly unsteady area) on the right in Figure 6. The area where the separation area or Karman vortices passed is shown in red and only the inside of this area is analyzed with LES. Thus, only the vortices generation area downstream from the separation can be analyzed with LES which is more suitable to the analysis of vortices.

The distribution of streamwise flow velocity and the distribution of vortices in the vicinity downstream from the blade are shown in **Figure 8**. Since the RANS-LES interface becomes more downstream than domain decomposition A, the reduction of the boundary layer resolution was controlled. In addition, as with domain decomposition A, the resolution of unsteady vortices from the blade trailing edge can be expected.

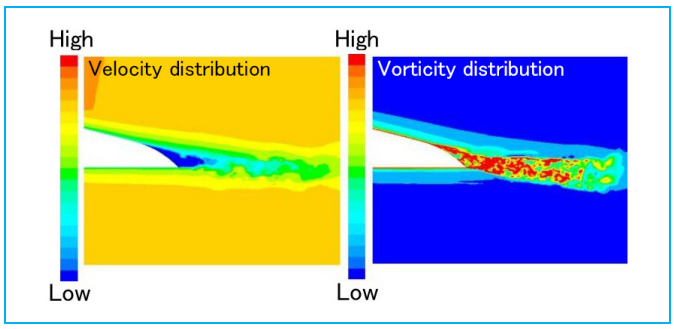

Figure 8 Analysis results of domain decomposition B (velocity distribution/vorticity distribution)
The estimation accuracy of the boundary layer is almost the same as RANS analysis (Figure 3). The problem where the boundary layer thickness is underestimated does not occur in this method, and the velocity distribution is closer to that of RANS analysis rather than the result of domain decomposition A. In the vorticity distribution, microscale vortices downstream from the blade have been analyzed. The vorticity distribution is not largely different from that by domain decomposition A (the right in Figure 5)

5.2 Comparison of analysis results

In ELES analysis using each domain decomposition, the time history of vertical flow velocity was observed at two points, specifically at 1% and 7% of the blade chord length downstream from the blade trailing edge. **Figure 9** shows the time history of flow velocity in domain decomposition A, and **Figure 10** shows the time history flow velocity in domain decomposition B. In both of the domain decompositions, unsteady vertical flow velocity fluctuation was observed at 7% downstream, and unsteady vortices passed through each observation point. On the other hand, there is a difference in the flow velocity fluctuation at 1% downstream from trailing edge of the blade. In domain decomposition A, more minute fluctuations were observed, while in domain decomposition B, more cyclical fluctuations were observed.

For the time history data of the vertical flow velocity fluctuations, a Fourier transform was conducted. A comparison of the respective ELES calculation results of the power spectra and the measurement data is shown in **Figure 11**. The peak and level at an Sh of 0.2 of the likely Karman vortices agree well with the measurement data especially in domain decomposition B where only the area downstream from the separation was subjected to LES analysis. On the other hand, in the

low-frequency and high-frequency areas, the spectra agree well with the measurement results at both observation points in domain decomposition A divided at 90% of the blade chord length, while in domain decomposition B, the spectrum in the high-frequency area tends to be low at the observation point 1% downstream from the trailing edge of the blade. In domain decomposition A, unsteady vortices are easily developed spatially because the LES region is located upstream of domain decomposition B. Whereas, in domain decomposition B, the distance from the RANS-LES interface to the observation point is small and we infer that unsteady vortices may not have been fully developed. However, a comparison of Figure 5 and Figure 8 shows that in domain decomposition A, the boundary layer from the 90% point to the separation point was analyzed as being less thick, while the upstream is set for LES. Therefore, there is a possibility that the RANS-LES interface is allocated as a trade-off between the estimation accuracy of the boundary layer and the resolving of unsteady vortices.

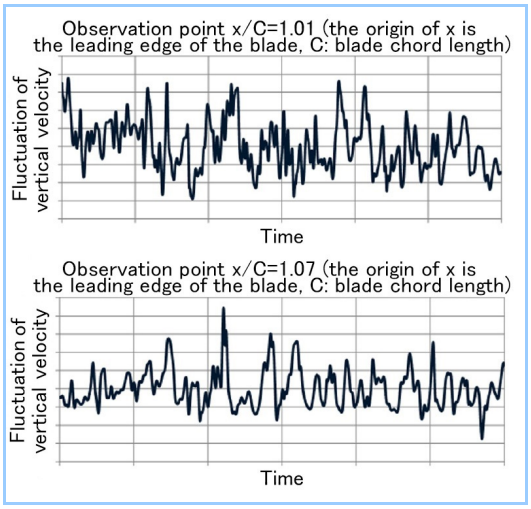

Figure 9 Analysis results of domain decomposition A (time history of vertical velocity around the trailing edge of the blade)

This shows the time history of velocity data at two observation points in domain decomposition A. In both observation points, macroscale fluctuations and microscale fluctuation were analyzed.

This indicates that vortices of various scales were generated. In the time history of velocity at x/C=1.01 shown in the above figure, the fluctuation of velocity at a higher frequency seems to be large.

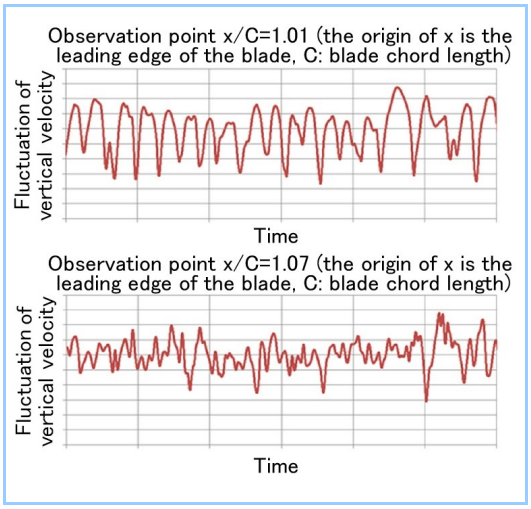

Figure 10 Analysis results of domain decomposition B (time-series flow velocity from the blade trailing edge)

This shows the time history of velocity data at two observation points in domain decomposition B. At the observation point far from the blade, the macroscale and the microscale fluctuations were analyzed.

This indicates that vortices of various scales were generated. In the analyzed velocity fluctuation at the observation point close to the blade shown in the above figure, there are fewer high-frequency components and slightly more periodical vortices than in the flow velocity fluctuation at the observation point far from the blade.

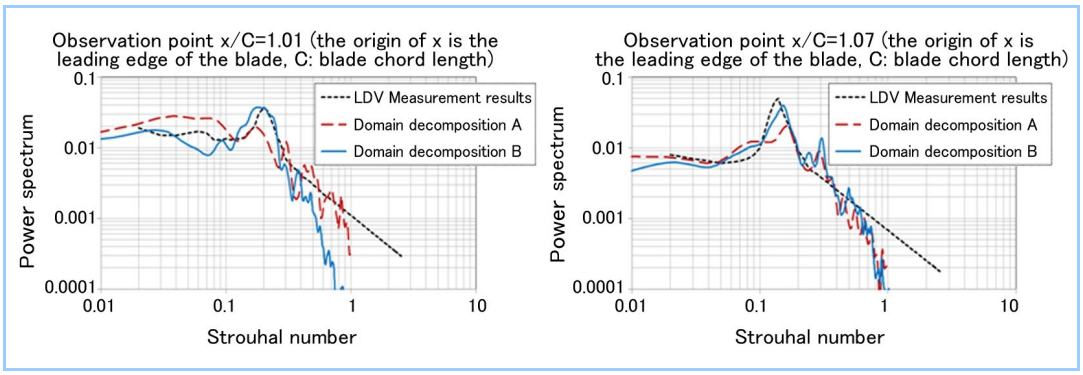

Figure 11 Comparison between the ELES analysis results and the measurement results

In the spectrum at the observation point of x/C=1.01 shown in the figure on the left, the peak level of domain decomposition B is closer to that of the measurement results and the spectrum in the zone at the larger Strouhal number of domain decomposition A is closer to the that of the measurement results. In the spectrum at the observation point of x/C=1.07 shown in the figure on the right, the peak level at the Strouhal number of 0.1 to 0.2 of domain decomposition B is closer to that of the measurement results, but there is no large difference between domain decomposition A and B in the spectrum in the zone at other Strouhal number..

6. Evaluation of domain decomposition

In the previous section, the ELES analysis results in the two kinds of domain decompositions conducted were compared, and it was found that in both of the domain decompositions, low-frequency and high-frequency vortices can be analyzed with high accuracy. Especially in domain decomposition B where only the area downstream from the separation was subjected to LES analysis, a spectrum waveform which indicates that Karman vortices were well captured was obtained, and it can be evaluated as an analysis method suitable for the estimation of singing noise.

In domain decomposition A separated at 90% of the blade chord length, although the peak of Karman vortices is weak, it can be evaluated as that the high frequency spectrum at the 1% trailing edge can be analyzed with higher accuracy than domain decomposition B.

In the comparison of the two domain decompositions shown in Figure 4 and Figure 7, it was found that there is a difference in the most upstream positions of the LES region. In domain decomposition A, the LES region starts upstream from the separation position, while in domain decomposition B, the LES region starts at the separation position. As shown in Figure 11, in domain decomposition B, the high frequency component is lower at 1% of the blade chord length downstream than in domain decomposition A, while the high frequency component is the same at 7% downstream. It seems that there is a possibility that microscale vortices with strong unsteadiness tend to increase while passing through the LES region in CFD analysis. In domain decomposition B, it seems that there is a possibility that vortices have not fully evolved because of the short LES region. Therefore, by starting the LES region at the more upstream position, the estimation accuracy of the spectrum in the high frequency area close to the blade trailing edge can be improved.

On the whole, it is considered that both of the domain decompositions are equal in analysis capability for vortices, but domain decomposition B, which evaluates the area using the fluid parameters, has a higher flexibility compared with other analysis subjects and operation conditions.

7. Conclusion

ELES analysis, which is a combination of RANS with a low calculation load and LES with a high calculation load, allows the high-accuracy analysis of unsteady vortices near the blade trailing edge with a relatively low calculation load. In particular, it is considered that domain decomposition which uses the fluid parameters for the decision of the interface has a high estimation accuracy of Karman vortices, which are the main cause of singing noise. Furthermore, this method has a high applicability to other analysis subjects and operation conditions. We will use ELES analysis for propeller design as a practical method for the estimation of trailing edge vortices, and improve the accuracy and develop a low noise propeller.

References

1. Bourgoyne, D.A., et al., Time averaged flow over a hydrofoil at high Reynolds number, Journal of Fluid Mechanics, Vol.496, (2003), pp. 365-404.
2. Bourgoyne, D.A., et al., Vortex shedding from a hydrofoil at high Reynolds number, Journal of Fluid Mechanics, Vol.531, (2005), pp. 293-324.
3. Davor Cokljat et al., Embedded LES Methodology for General-Purpose CFD Solvers". Proc. Turbulent Shear Flow Phenomena, Proc. 6th Int. Symp. Turbulence and Shear Flow Phenomena, (2009), pp. 1191-1196.
4. Takuyoshi Yamada, et al., Study on the Calculation Method for Unsteady Vortex from Trailing Edge of Blade, AICFM13, Vol.13, (2015), AICFM13-219.